M. QUINTEN✉

Local fields close to the surface of nanoparticles and aggregates of nanoparticles

Mauritiusstrasse 7, 52457 Aldenhoven, Germany

ABSTRACT A refined discussion of the near-field scattering of spherical nanoparticles and the electromagnetic fields close to the particle surface is given. New results for the dependence on the distance from the surface and the angular distribution of the scattered light in the near-field are given. It will be shown that the radial component of the electric field leads to striking differences in the phase functions in the near-field and the far-field. Exemplary computations are presented for Ag and Au particles with different size. In a second part the discussion is extended to assemblies of spherical Ag and Au nanoparticles. It will be shown that large near-fields at wavelengths commonly used in SERS experiments are obtained for aggregates. In the near-field scattering intensity "hot spots" mark regions between particles in the aggregate where the near-field is particularly high.

PACS 42.25.Bs; 78.66.Vs; 82.70.Dd

1 Introduction

Measuring absorption of light and elastic light scattering has turned out to be a useful tool to examine samples containing small particles. In common experimental setups and in technical applications the measurements are carried out in the far-field zone, i.e. far away from the surfaces of the particles. However, in SERS (surface enhanced Raman scattering) the large local electromagnetic fields on the surface or in the vicinity of a small particle or an aggregate of particles are used to enhance Raman scattering of light by adsorbed molecules (see for instance [1–5]). Such enlarged electromagnetic fields also play an important role for nonlinear optical properties of small particles (e.g. [6]), or in guiding light along nanostructures [7]. The optical near-field is also a central topic in scanning near-field optical microscopy (SNOM), where evanescent waves are used. As such waves are spatially restricted, the scattering of evanescent waves by small particles is best for nanoparticles on the surface where the evanescent wave is generated by, e.g. total internal reflection. Some results for homogeneous and coated particles and for aggregates of spherical particles were recently published ([8–11] and references therein).

✉ E-mail: ulmi.quinten@t-online.de

Elastic light scattering and absorption by single spherical particles was already solved in 1908 by Mie [12]. The solution is based upon the expansion of the incident wave, the scattered wave and the wave interior of the particle into corresponding vector spherical harmonics. The extinction and scattering cross-sections of the spherical particle follow from the calculation of the total absorption rate according to Poynting's theorem. In addition to these quantities Messinger et al. [13] introduced new quantities: near-field efficiencies, which are a measure for the spatially averaged square of the electric field. Messinger et al. [13] discussed the wavelength dependence of the near-field efficiencies at distance $R = a$, i.e. at the surface of the particle, for Ag, Au and Cu clusters of various sizes. In 1995 Quinten [14] extended the theory also to the magnetic field of the scattered wave and discussed the dependence of the near-field efficiency on cluster size and the distance from the cluster surface, including the Poynting vector of the scattered wave. The aim of this paper is to give a refined discussion of the near-field scattering of spherical particles. New results for the dependence on the distance from the cluster surface and the angular distribution of the scattered light in the near-field are obtained. For that purpose the efficiencies and the phase functions are discussed. It will be shown that the radial component of the electric field determines the electric field in the vicinity of the cluster, leading to striking differences in the phase functions in the near-field and the far-field. In a second part this discussion is extended to aggregates of spherical particles. The far-field optical cross-sections of aggregates can be calculated according to the model of Gérardy and Ausloos [15]. In this model the coherent superposition of the electromagnetic fields of all scattered waves in the near-field determines the total cross-sections for extinction and scattering of light by the aggregate. It is therefore a rather simple task to calculate also the field intensities in the vicinity of the particles in an aggregate. The cross sections and the near-field intensities will be discussed for exemplary gold nanoparticle aggregates.

2 Theory

2.1 *Single particles*

The description of the light scattering by spherical particles is based upon the expansion of all electromagnetic waves into spherical partial waves using vector spherical

harmonics, and applying Maxwell's boundary conditions to resolve the unknown expansion coefficients of the scattered and interior wave. From Poynting's law the power rates for absorption and scattering are determined. These rates are normalized on the intensity I_0 of the incident wave to obtain the optical cross-sections σ_{ext} and σ_{sca} for extinction (absorption plus scattering) and scattering. For better comparison in the following, it is convenient to normalize these quantities on the geometrical cross-section of a sphere with diameter $2a$ to obtain the dimensionless extinction and scattering efficiencies Q:

$$Q_{\text{ext}} = \frac{2}{(ka)^2} \sum_{n=1}^{\infty} (2n+1)\,\text{Re}\,(a_n + b_n)\;, \tag{1}$$

$$Q_{\text{sca}} = \frac{2}{(ka)^2} \sum_{n=1}^{\infty} (2n+1)\left(|a_n|^2 + |b_n|^2\right)\;. \tag{2}$$

The quantity $k = (2\pi n_{\text{M}}(\lambda))/\lambda$ is the wavenumber outside the particle in the surrounding medium M with refractive index n_{M}. The quantities a_n and b_n are the scattering coefficients of the sphere and Re means the real part.

In a previous publication [14] it has been shown that these quantities are identical in the near-field and in the far-field. Hence, Q_{ext} and Q_{sca} solely are a measure for the ability to extinguish and to scatter an electromagnetic wave at incident wavelength λ to a certain amount. They do not provide information about the strength of the electromagnetic fields nearby or far from the particle at distance $R \geq a$ from particle center. This information is contained in the near-field efficiencies Q_{NF} and Q_R:

$$Q_{\text{NF}}(R) = \frac{R^2}{\pi a^2 I_0} \int_0^{2\pi} \int_0^{\pi} \left(\boldsymbol{E}_{\text{sca}}(R)\boldsymbol{E}_{\text{sca}}^*(R)\right) \sin\theta \, d\theta \, d\varphi\;, \tag{3}$$

$$Q_R(R) = \frac{R^2}{\pi a^2 I_0} \int_0^{2\pi} \int_0^{\pi} \left(\boldsymbol{E}_{\text{r,sca}}(R)\boldsymbol{E}_{\text{r,sca}}^*(R)\right) \sin\theta \, d\theta \, d\varphi\;, \tag{4}$$

introduced in 1981 by Messinger et al. [13]. Q_{NF} represents the square of the spatially averaged electric field of the scattered wave, and Q_R represents the square of only the spatially averaged radial component E_{r} of the electric field of the scattered wave, which is included in Q_{NF}. It is mainly this radial component, E_{r}, that determines the difference between the far-field and the near-field. E_{r} is excluded from the energy flux of the scattered wave, and therefore from Q_{sca}. Q_{NF} is larger than Q_{sca} in the near-field zone because E_{r} increases with R^{-2} faster than with R^{-1} as one moves from far-field to the surface of the particle. For large R, Q_{NF} decreases to the asymptotic value Q_{sca} and Q_R vanishes, because E_{r} now decreases with R^{-2} faster than with R^{-1}. The explicit calculation of Q_{NF} and Q_R yields

$$Q_{\text{NF}}(R) = 2\frac{R^2}{a^2} \sum_{n=1}^{\infty} \left\{ |a_n|^2 \left[(n+1) \left| h_{n-1}^{(1)}(kR) \right|^2 \right.\right.$$
$$\left.\left. + n \left| h_{n+1}^{(1)}(kR) \right|^2 \right] + (2n+1)\,|b_n|^2 \left| h_n^{(1)}(kR) \right|^2 \right\}\;, \tag{5}$$

$$Q_R(R) = \frac{2}{(ka)^2} \sum_{n=1}^{\infty} (2n+1)(n+1)n\,|a_n|^2 \left| h_n^{(1)}(kR) \right|^2\;, \tag{6}$$

where $h_n^{(1)}$ are spherical Hankel functions of first kind and order n.

Messinger et al. [13] discussed the wavelength dependence of these quantities at distance $R = a$, i.e. at the surface of the spherical particle, for Ag, Au and Cu clusters of various sizes. In 1995 Quinten [14] extended the theory also to the magnetic field of the scattered wave and discussed the dependence of Q_{NF} on cluster size, distance $D = R - a$ from the cluster surface and wavelength of the incident light. It was shown that the local electric and magnetic field of the scattered wave are strongly enlarged in the vicinity of the spherical particle, and that giant enhancements in the ratio $Q_{\text{NF}}/Q_{\text{sca}}$ are obtained for very small particles independently of the particle material. In this paper a refined discussion of Q_{NF} and a discussion of Q_R in dependence on R or D, respectively, will be given for spherical clusters.

Moreover, the phase functions that describe the angular distribution of the scattered light are discussed in more detail. Within the framework of Mie's theory it is common to express the scattering efficiency by introducing phase functions $S_1(\theta)$ and $S_1(\theta)$ perpendicular and parallel to the scattering plane, so that

$$Q_{\text{sca}} = \frac{R^2}{\pi a^2 I_0} \int_0^{2\pi} \int_0^{\pi} \left(I_1(\theta)\sin^2\varphi + I_2(\theta)\cos^2\varphi\right) \sin\theta \, d\theta \, d\varphi\;, \tag{7}$$

with

$$I_1(\theta) = \frac{I_0}{(kR)^2} |S_1(\theta)|^2$$
$$= \frac{I_0}{(kR)^2} \left| \sum_{n=1}^{\infty} \frac{2n+1}{n(n+1)} (a_n \pi_n(\theta) + b_n \tau_n(\theta)) \right|^2 \tag{8}$$

$$I_2(\theta) = \frac{I_0}{(kR)^2} |S_2(\theta)|^2$$
$$= \frac{I_0}{(kR)^2} \left| \sum_{n=1}^{\infty} \frac{2n+1}{n(n+1)} (a_n \tau_n(\theta) + b_n \pi_n(\theta)) \right|^2\;. \tag{9}$$

The angle-dependent functions $\tau_n(\theta)$ and $\pi_n(\theta)$ are defined as $\tau_n(\theta) = \partial P_{n1}/\partial\theta$ and $\pi_n(\theta) = P_{n1}/\sin\theta$. $P_{n1}(\cos\theta)$ are associated Legendre polynomials for $m = 1$.

$I_1(\theta)$ and $I_2(\theta)$ give detailed information about the angular distribution of the scattered light in the far field. However, in the near-field the R-dependence is different from $1/(kR)^2$. For discussion of the near-field behavior, R-dependent phase functions $s_1(\theta)$ and $s_2(\theta)$, respectively, intensities $i_1(\theta)$ and $i_2(\theta)$ must be introduced. They are defined as

$$i_1(\theta) = |s_1(\theta)|^2 = I_0 \left| e_\varphi(\theta) \right|^2 \tag{10}$$

$$i_2(\theta) = |s_2(\theta)|^2 = I_0 \left\{ |e_\theta(\theta)|^2 + |e_r(\theta)|^2 \right\}\;, \tag{11}$$

with e_r, e_θ and e_φ being the normalized components of the electric field vector in spherical coordinates. The R-dependence is included in these field components. For $R \gg a$,

i.e. in the far-field zone, it is

$$I_1(\theta) = \lim_{R \gg a} i_1(\theta) \,, \tag{12}$$

$$I_2(\theta) = \lim_{R \gg a} i_2(\theta) \,. \tag{13}$$

The definition of $i_1(\theta)$ and $i_2(\theta)$ follows from (3) using the multipole expansion of the scattered electric field. Therefore, the radial field component E_r only contributes to $i_2(\theta)$.

2.2 *Aggregates*

The theory of extinction and scattering by aggregates of spherical particles with arbitrary topology according to Gérardy and Ausloos [15] is used to calculate cross-section spectra of various gold nanoparticle aggregates. In this theory, the electromagnetic fields of the scattered waves of all neighboring particles are taken into account for each of the N particles in the aggregate. Then, Maxwell's boundary conditions yield a set of linear equations for the expansion coefficients $\alpha_{nm}(i)$ and $\beta_{nm}(i)$ of the scattered wave of particle i:

$$\alpha_{nm}(i) = \exp(\mathrm{i} \boldsymbol{k} \boldsymbol{r_i}) a_n(i)$$
$$+ a_n(i) \sum_{j \neq i}^{N} \sum_{q=1}^{\infty} \sum_{p=-q}^{q} \alpha_{qp}(j) S_{nmqp}(i, j) + \beta_{qp}(j) T_{nmqp}(i, j) \,,$$
$$\tag{14}$$

$$\beta_{nm}(i) = \exp(\mathrm{i} \boldsymbol{k} \boldsymbol{r_i}) b_n(i)$$
$$+ b_n(i) \sum_{j \neq i}^{N} \sum_{q=1}^{\infty} \sum_{p=-q}^{q} \alpha_{qp}(j) T_{nmqp}(i, j) + \beta_{qp}(j) S_{nmqp}(i, j) \,.$$
$$\tag{15}$$

The coefficients $a_n(i)$ and $b_n(i)$ are the scattering coefficients of the single isolated sphere i for the TM-mode and TE-mode of order n, following from Mie's theory [12]. The matrix elements $S_{nmqp}(i, j)$ and $T_{nmqp}(i, j)$ take into account the topology of the aggregate, i.e. the relative spherical coordinates d_{ij}, θ_{ij} and φ_{ij} of particle j in the coordinate frame of particle i. They decrease with increasing center-to-center distance d_{ij} and become negligible at sufficiently large distances d_{ij}. Then, $\alpha_{nm}(i)$ and $\beta_{nm}(i)$ reduce to $a_n(i)$ and $b_n(i)$, except for the phase factor $\exp(\mathrm{i} \boldsymbol{k} \boldsymbol{r_i})$ which accounts for the phase of the incident wave at the site of particle i.

The extinction and scattering cross-sections of the aggregate follow as

$$C_{\text{ext}}(N) = \frac{2\pi}{k^2} \sum_{i=1}^{N} \sum_{n=1}^{\infty} \sum_{m=-n}^{n} \text{Re} \left\{ \alpha_{nm}(i) + \beta_{nm}(i) \right\} \,, \tag{16}$$

$$C_{\text{sca}}(N) = \frac{2\pi}{k^2} \sum_{i=1}^{N} \sum_{n=1}^{\infty} \sum_{m=-n}^{n} |\alpha_{nm}(i)|^2 + |\beta_{nm}(i)|^2$$
$$+ \frac{2\pi}{k^2} \sum_{i=1}^{N} \sum_{n=1}^{\infty} \sum_{m=-n}^{n} \text{Re} \left\{ \alpha_{nm}^*(i) \left(1 - \frac{\alpha_{nm}(i)}{a_n(i)} \right) \right.$$
$$\left. + \beta_{nm}^*(i) \left(1 - \frac{\beta_{nm}(i)}{b_n(i)} \right) \right\} \,. \tag{17}$$

Extinction and scattering of light by an arbitrary N-sphere aggregate not only depend on the sizes of the primary particles, the size and topology of the aggregate and the particle materials, but also on the polarization and the propagation direction of the incident wave. Hence, it seems appropriate in the following to take an average over different angles of incidence and polarizations to obtain results for unpolarized light.

For calculating the near-field intensities, the electromagnetic fields of the scattered waves of all particles are added up in a point P with position $\boldsymbol{r}$

$$\boldsymbol{E}(\boldsymbol{r}) = \sum_{i=1}^{N} \boldsymbol{E}_{\text{sca}}^i(\boldsymbol{r}) \tag{18}$$

The intensity in P is then proportional to $|\boldsymbol{E}(\boldsymbol{r})|^2$.

3 Numerical results for single particles
3.1 *Efficiencies*

Large enhancement factors $Q_{\text{NF}}/Q_{\text{sca}}$ are obtained for very small particles. This follows from Fig. 1, showing $Q_{\text{NF}}/Q_{\text{sca}}$ in dependence on the particle size for particles smaller than $2a = 400$ nm at a fixed wavelength $\lambda = 514.5$ nm. Giant electric fields of the scattered wave are obtained for particles smaller than $2a = 20$ nm. This result for $Q_{\text{NF}}/Q_{\text{sca}}$ is independent of the particle material, however, for metal particles Q_{sca} is already much bigger than for dielectric clusters of same size. Then, Q_{NF} also approaches very large values. A further increase is obtained for distinct metals for which nanoparticles exhibit a surface plasmon polariton resonance, e.g. Au- Ag- or Cu-clusters. In these resonances Q_{sca} is much bigger than at off-resonance wavelengths. For example, a silver cluster in air with diameter $2a = 20$ nm exhibits a surface plasmon resonance at $\lambda = 367$ nm. This is, however, the position of the maximum absorbance due to the particle with an efficiency of $Q_{\text{abs}} = 1.8248$. In the scattering efficiency the maximum value of Q_{sca} is obtained at $\lambda = 372$ nm, amounting to $Q_{\text{sca}} = 1.8978 \times 10^{-2}$ (a factor 100 (!) smaller than the absorption). At $\lambda = 514$ nm (off-resonance), Q_{sca} amounts to $Q_{\text{sca}} = 1.1349 \times 10^{-3}$. In contrast, for a silica cluster of $2a = 20$ nm they amount to $Q_{\text{sca}}(372 \text{ nm}) = 1.7133 \times 10^{-4}$ and $Q_{\text{sca}}(514 \text{ nm}) = 4.4961 \times 10^{-5}$.

Giant electromagnetic fields as obtained for particles smaller than $2a = 20$ nm should give rise to strong enhancements in, e.g. Raman scattering of chemisorbed molecules at cluster surfaces. However, the Raman intensity in surface enhanced Raman scattering (SERS) is the product of electromagnetic effects and molecular effects. Only if the inelastically scattered light is in resonance with the local field of the particles, is the reradiation efficiency of the adsorbed molecules also enhanced. Therefore, the largest enhancements in SERS are not necessarily obtained for the smallest particles, as discussed in [2, 3].

Figure 2 depicts the wavelength dependence of Q_{NF}, Q_R and Q_{sca} for clusters of Au and Ag with diameter $2a = 10$ nm at distance $R = a$, i.e. at the surface of the particle ($D = 0$). The optical constants of Au and Ag are taken from [16]. For better comparison Q_{sca} is multiplied by the given factors. It can be seen that Q_{NF} and Q_R exhibit similar spectral
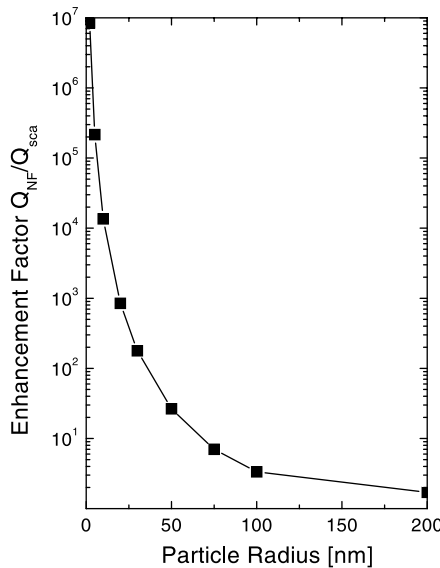
FIGURE 1   Enhancement factor of the local electric field of the scattered wave in dependence upon the particle size at wavelength $\lambda = 514.5$ nm

features as Q_{sca}, interband transitions at short wavelengths and a surface plasmon polariton resonance. However, there are also clear differences. First, the wavelengths with maximum Q_{NF} and Q_R are slightly redshifted compared to the wavelength at which Q_{sca} is maximum. In detail, Q_{sca} is maximum at $\lambda = 514$ nm and $\lambda = 371$ nm for the Au and Ag cluster, respectively, whereas Q_{NF} and Q_R are maximum at $\lambda = 522$ nm and $\lambda = 375$ nm, respectively. Moreover, it becomes obvious that in the interband transition region, the near-field efficiencies are almost wavelength-independent, in contrast to Q_{sca}. At longer wavelengths the near-field efficiencies decrease more slowly than Q_{sca} because the scattering of light by small particles depends on the ratio of particle circumference/wavelength. Then, the effect of an increasing wavelength is similar to the effect of a decreasing particle size at fixed wavelength, as illustrated in Fig. 1. Therefore, the decrease in Q_{NF} and Q_R with increasing wavelength must be

slower than that of Q_{sca}. Indeed, they become approximately constant for large wavelengths. In general, it can be seen that Q_R is the main contribution to Q_{NF}. Q_R amounts to 67% of Q_{NF} for $R = a$. That means that in the near-field the electric field is dominated by the radial component, which is very large.

In Fig. 3 series of spectra of Q_{NF}, Q_R and Q_{sca} are given for Au-clusters with particle sizes $2a = 10, 20, 40, 100, 150$ and 200 nm. The conclusions from Fig. 2 can also be drawn from this figure. The spectral dependence of the efficiencies changes when the particle size is increased, since, for larger particles, multipoles higher than the dipole contribute to the scattered and interior field of the clusters. This leads to the obvious broadening of the plasmon resonance for larger particles. In a first rough approximation the multipole of order n is resonant at the condition

$$\left| \varepsilon(\lambda) + \frac{n+1}{n} \varepsilon_M \right|^2 = \text{minimum} . \tag{19}$$

The quantities ε and ε_M are the dielectric functions of the cluster material and the surrounding matrix material. The best-known is the dipole resonance ($n = 1$) at $\varepsilon \approx -2\varepsilon_M$, which corresponds to the surface plasmon polariton in Fig. 2. From the dispersion of $\varepsilon(\lambda)$ of Au it follows that for larger Au-particles the dipole resonance is redshifted followed by the other multipoles at smaller wavelengths.

A further result is that with increasing particle size the enhancement of the near-field decreases compared to that of the far-field. For the largest particle under consideration with $2a = 200$ nm, Q_{NF} approximately amounts to only $Q_{NF} \approx Q_{sca}$ in the whole spectral region.

In Fig. 4 the dependence of Q_{NF} and Q_R on the distance $D = R - a$ from the particle surface are shown for a gold cluster with $2a = 100$ nm at two wavelengths $\lambda_1 = 514.5$ nm and $\lambda_2 = 780$ nm. For comparison Q_{sca} is given as a horizontal line. The behavior of Q_{NF} and Q_R is similar for both wavelengths. Very close to the surface, Q_R is the dominant contribution to Q_{NF}. With increasing distance both quan-
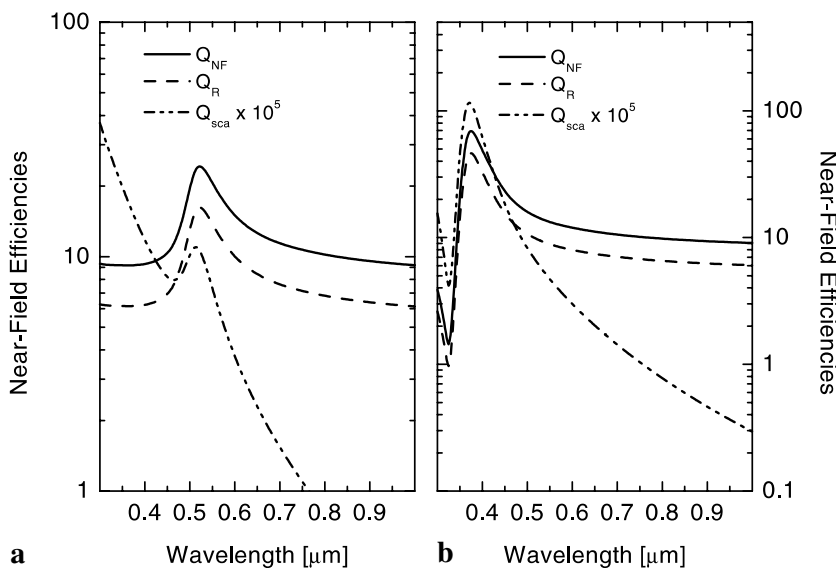

FIGURE 2   Spectral dependence of Q_{NF}, Q_R and Q_{sca} for a spherical metal cluster with diameter $2a = 10$ nm for gold (**a**), silver (**b**). The optical constants are taken from [13]
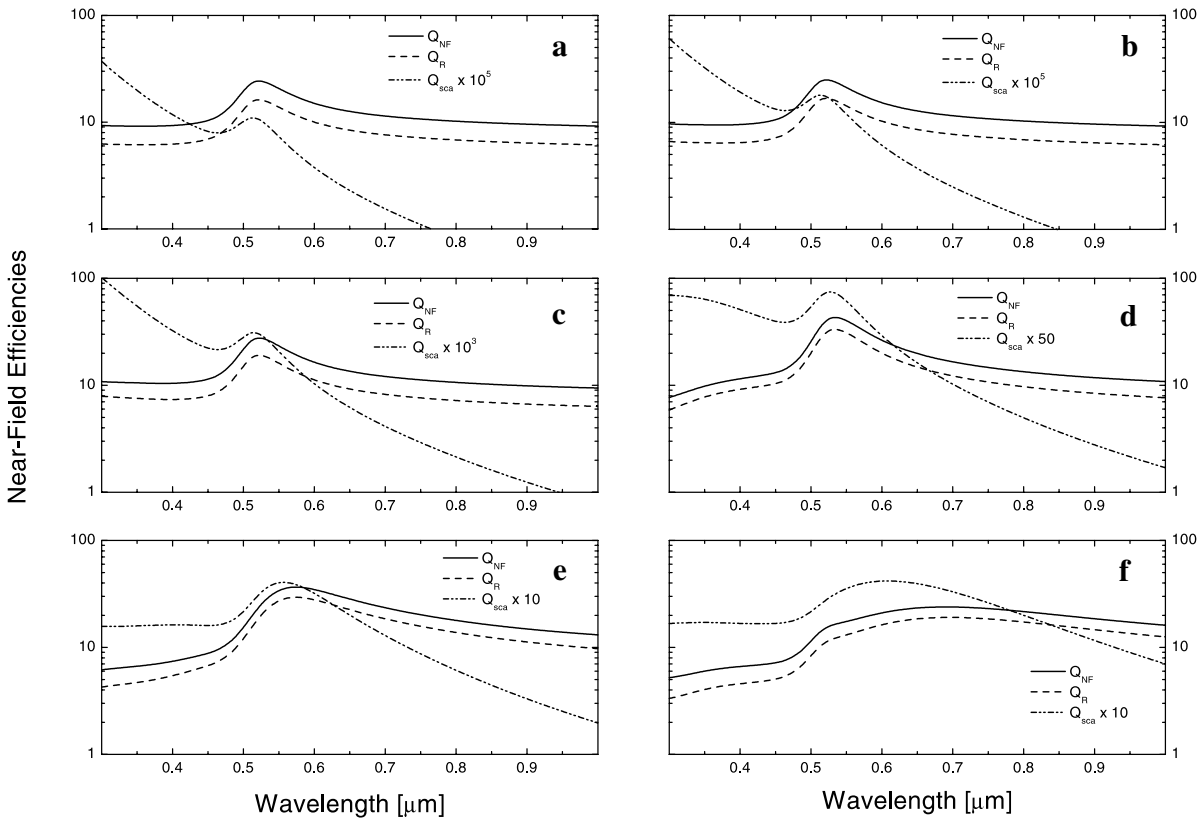
FIGURE 3 Size dependence of spectra of Q_{NF}, Q_R and Q_{sca} for a spherical gold clusters with increasing diameter: $2a = 10$ nm (**a**), $2a = 20$ nm (**b**), $2a = 40$ nm (**c**), $2a = 100$ nm (**d**), $2a = 150$ nm (**e**), $2a = 200$ nm (**f**)
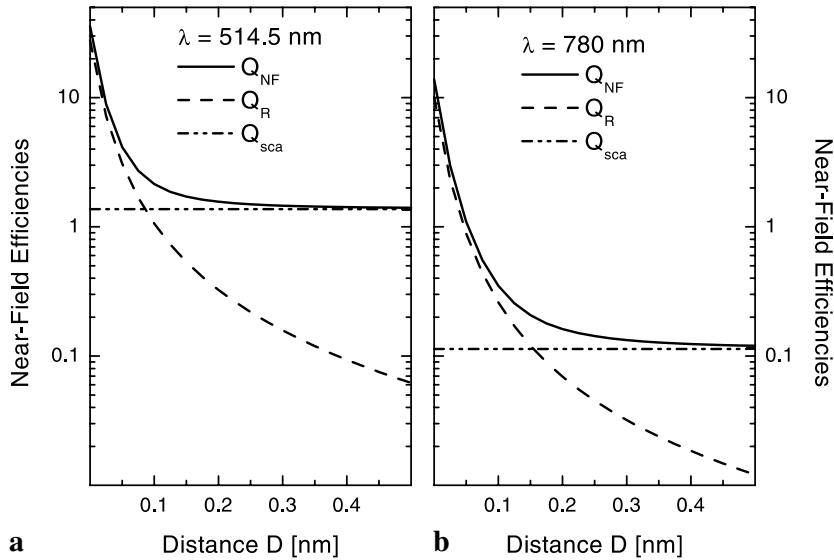

FIGURE 4 Dependence of Q_{NF}, Q_R and Q_{sca} on the distance D from the cluster surface for gold clusters with $2a = 100$ nm at wavelength $\lambda = 514.5$ nm (**a**) and at wavelength $\lambda = 780$ nm (**b**)

tities decrease. While Q_{NF} approaches Q_{sca}, Q_R decreases more rapidly and amounts to about 1/20 of Q_{sca} at a distance of $D = 0.5\,\mu$m, corresponding in the present example to $D = 10a$. Also for smaller particles, many further calculations showed that at $D = 0.5\,\mu$m Q_R has decreased to approximately 1/20 of Q_{sca}, and, hence, becomes negligible. For the gold particle under consideration Q_R is in the order of Q_{sca} at $D = 0.076\,\mu$m $= 3a$ for $\lambda_1 = 514.5$ nm and $D = 0.15\,\mu$m $= 6a$ for $\lambda_2 = 780$ nm.

For a more quantitative discussion of Figs. 1, 2 and 4 we assume particle sizes as small compared to the wavelength, as the main contribution to the efficiencies in (2), (5) and (6) is given by the dipole ($n = 1$). Then, it follows from (2) that

$$Q_{sca} = \frac{6|a_1|^2}{(ka)^2}, \tag{20}$$

and from (5)

$$Q_{\mathrm{NF}} = \frac{6|a_1|^2}{(ka)^2} \frac{(kR)^2}{3} \left(2 \left| h_0^{(1)}(kR) \right|^2 + \left| h_2^{(1)}(kR) \right|^2 \right) , \qquad (21)$$

and from (6)

$$Q_R = \frac{6|a_1|^2}{(ka)^2} 2 \left| h_1^{(1)}(kR) \right|^2 . \qquad (22)$$

The TM-dipole a_1 is in this approximation given as

$$a_1 = \frac{2}{3} \mathrm{i}(ka)^3 \frac{\varepsilon(\lambda) - \varepsilon_{\mathrm{M}}(\lambda)}{\varepsilon(\lambda) + 2\varepsilon_{\mathrm{M}}(\lambda)} \qquad (23)$$

with ε and ε_{M} being the dielectric functions of the particle material and the surrounding matrix M. Note that in these equations we only take into account the contribution of the TM-dipole a_1, which exhibits the surface plasmon resonance. The TE-dipole b_1 is in the order of the TM quadrupole a_2 and can be neglected. Furthermore, for nanoparticles it does not exhibit a resonance. It is obvious from (21) and (22) that in this approximation the behavior of the Hankel-functions $h_0^{(1)}$, $h_1^{(1)}$ and $h_2^{(1)}$ determines the values of Q_{NF} and Q_R with respect to Q_{sca} for all wavelengths and all particle sizes (as long as the particles are small compared with the wavelength). For small arguments kR, i.e. close to the surface of the particle, the Hankel-functions become approximately

$$h_n^{(1)}(kR) \approx \frac{\Gamma(0.5)}{2\Gamma(n+1.5)} \left(\frac{kR}{2} \right)^n - \mathrm{i} \frac{\Gamma(n+0.5)}{2\Gamma(0.5)} \left(\frac{2}{kR} \right)^{n+1} . \qquad (24)$$

The function $\Gamma(m)$ is the Gamma function. For large arguments kR they become approximately

$$h_n^{(1)}(kR) \approx (-\mathrm{i})^{n+1} \frac{\exp(\mathrm{i}kR)}{kR} . \qquad (25)$$

Within this approximation it is easy to show that for large arguments, kR, the near-field efficiencies become $Q_{\mathrm{NF}} = Q_{\mathrm{sca}}$ and $Q_R = 0$. Furthermore, at a fixed wavelength λ the value $Q_R = Q_{\mathrm{sca}}/20$ is always obtained for the same distance R, independently of the particle size as already mentioned in the discussion of Fig. 4. On the other hand, the distance R where $Q_R = Q_{\mathrm{sca}}/20$ depends on the wavelength. When this value is approached for λ_1 at a distance R_1, it is obtained at R_2 for wavelength λ_2 with $R_1/\lambda_1 = R_2/\lambda_2$.

Small arguments kR can be obtained either for distances R close to the particle surface, i.e. $R \approx a$, or for long wavelengths, i.e. small wavenumbers k. For example, for a particle with $2a = 20$ nm and $R = a$, the enhancement $Q_{\mathrm{NF}}/Q_{\mathrm{sca}}$ amounts to 13 544 which is in very good agreement with the exact value of 13 587 in Fig. 1. Since for small arguments kR due to large wavelengths $Q_{\mathrm{NF}} \approx 3Q_{\mathrm{sca}}/(kR)^4$ and $Q_R \approx 2Q_{\mathrm{sca}}/(kR)^4$, both become approximately constant as already seen in Fig. 2. The decrease of Q_{sca} proportional to $1/\lambda^4$ is counteracted by the increase of $1/(kR)^4$ with λ^4. Moreover, the ratio Q_R/Q_{NF} approaches the value 0.67, as obtained in the evaluation of Fig. 2.

3.2   *Phase functions*

For discussion of the phase functions, the angular distribution of the scattered intensities perpendicular (azimuthal angle $\varphi = 90°$, I_1 and i_1) and parallel ($\varphi = 0°$, I_2 and i_2) to the plane of incidence is plotted in Fig. 5 for a gold particle with diameter $2a = 100$ nm for distances up to $R = 5a$. $i_1(\theta)$ and $i_2(\theta)$ are compared with $I_1(\theta)$ and $I_2(\theta)$. Note that the results for I_1 and I_2 in the near-field are obtained using the formulae (8) and (9) which are valid only in the far-field zone. The hatched spherical region in the center of each plot corresponds to the cluster. The intensities are plotted with a logarithmic scale.

$I_1(\theta)$ and $I_2(\theta)$ obviously correspond to the intensity distribution expected for a dipole in the far-field, i.e. $I_1(\theta)$ independent of the angle θ, and $I_2(\theta)$ proportional to $(\cos\theta)^2$. That means that the scattering of light by this particle at wavelength $\lambda = 514.5$ nm is still dominated by the dipole mode in the multipolar expansion of the scattered wave. This is in agreement with the result for the total scattering cross-section in Fig. 3d. $i_1(\theta)$ is rather similar to $I_1(\theta)$ except that the magnitudes are increased by a factor 7 close to the particle surface. At $R = 5a$ the intensities are of comparable magnitude. In contrast, $i_2(\theta)$ completely differs from $I_2(\theta)$. Close to the particle surface the near-field intensity is increased by a factor 40. At $R = 5a$ the intensities are of comparable magnitude, because of the contribution of the radial component E_r of the electric field that only contributes to $i_2(\theta)$ (see again (13)). As already shown above in Fig. 4, this contribution becomes negligible just at $R = 10a$ for the gold particle with $2a = 100$ nm. More significant than the differences in the magnitudes is the completely different angular distribution of the near-field intensity compared to the far-field intensity. In the far-field, the intensity $I_2(\theta)$ is proportional to $(\cos\theta)^2$ and, hence, exhibits minima at $\theta = \pm 90°$. In contrast, in the near-field these minima have vanished and the intensity at $\theta = \pm 90°$ is even larger than those at $\theta = 0°$ and $\theta = 180°$. For further discussion it seems appropriate to divide $i_2(\theta)$ in the two contributions from the field components e_θ and e_r. Then, it can be expected that the contribution $|e_\theta|^2$ will be similar to $I_2(\theta)$. This division is made in Fig. 6. As can be seen from this figure, actually, the contribution $|e_\theta|^2$ is rather similar to $I_2(\theta)$, except for the magnitude, which is increased by a factor 7 close to the particle surface, similar to i_1 in comparison with I_1. The contribution of the radial field component $|e_r|^2$ is 6 times larger than $|e_\theta|^2$. Therefore, the near-field scattering pattern is dominated by the radial component. However, the most significant feature is that the angular distribution of $|e_r|^2$ is obviously perpendicular to that of $|e_\theta|^2$ in the plane of incidence. Then, the sum $|e_\theta|^2 + |e_r|^2$ is maximum at $\theta = \pm 90°$ and is minimum at $\theta = 0°$ and $\theta = 180°$, as already shown in Fig. 5d.

4   Numerical results for aggregates

In this section we report on numerical results for planar silver and gold nanoparticle aggregates with $N = 9$, 13 and 16 primary particles with diameter $2a = 50$ nm, as illustrated in Fig. 7. Efficiency spectra and in addition the scattering enhancement $Q_{\mathrm{sca}}(N)/(N^* Q_{\mathrm{sca}}(1))$ are compiled
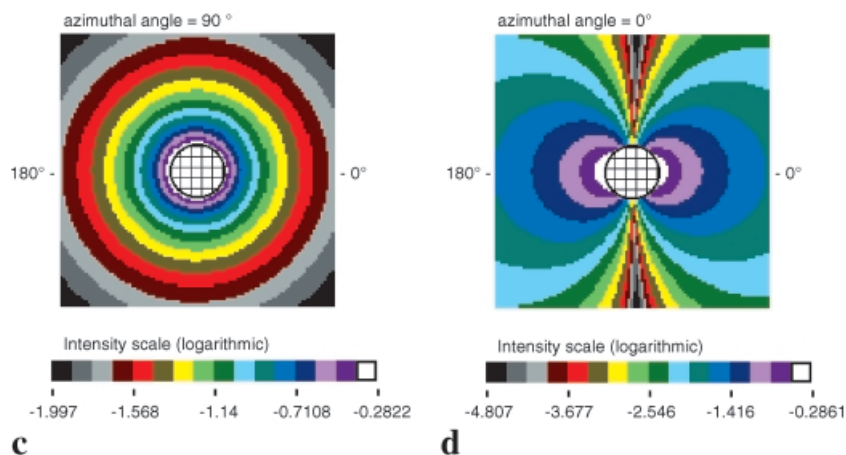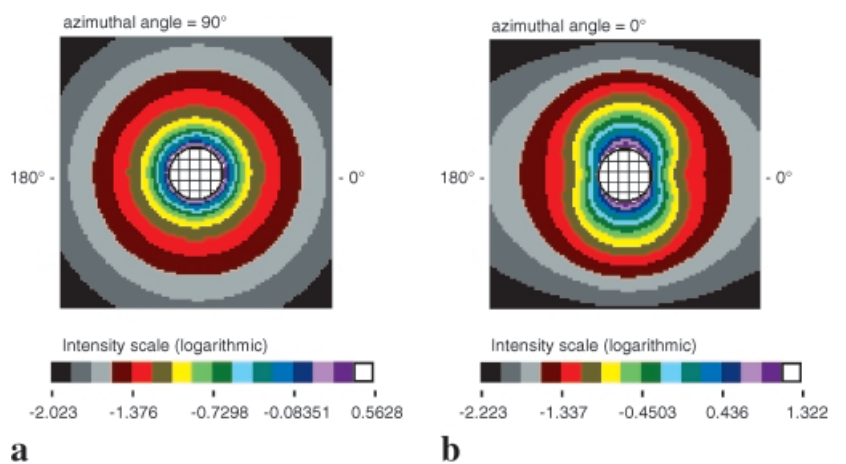
FIGURE 5 Angular distribution of the intensity of the light scattered by a spherical gold particle with diameter $2a = 100$ nm. **a** Perpendicular to the plane of incidence, near-field, i_1. **b** In the plane of incidence, near-field, i_2. **c** Perpendicular to the plane of incidence, far-field, I_1. **d** In the plane of incidence, far-field, I_2
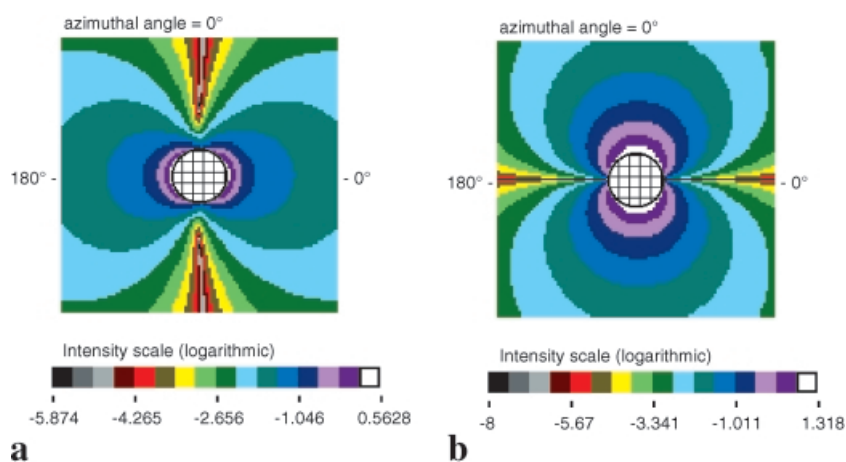
FIGURE 6 Contributions of E_r and E_θ to the intensity i_2 in the plane of incidence for the gold particle in Fig. 5. **a** Contribution of E_θ. **b** Contribution of E_r

in Fig. 8 for silver, and in Fig. 9 for gold. The spectra are calculated for unpolarized incident light. In addition near-field intensities at wavelength $\lambda = 830$ nm are given for the gold nanoparticle particle aggregate with $N = 16$ primary particles in Fig. 10.

Beginning with the spectra of the silver aggregates on the left side of Fig. 8, the effect of aggregation of nanoparticles is clearly recognizable. Compared to the spectrum of N isolated particles, the corresponding N-particle aggregate exhibits additional extinction features at longer wavelengths λ where the surface plasmon of the single particle is strongly

decreased. In the spectral region of the surface plasmon, the extinction by the aggregate is decreased. Moreover, it can be seen that at long wavelengths the scattering is the main contribution to the extinction, also for the single particles, whereas at short wavelengths the absorption dominates the extinction. For the single particle the scattering can be described by Rayleigh scattering, i.e. it is proportional to $1/\lambda^4$. The additional extinction features are due to the electromagnetic coupling among the primary particles in the aggregate. This coupling yield a splitting of the plasmon resonance of the primary particle in several new resonances, the number
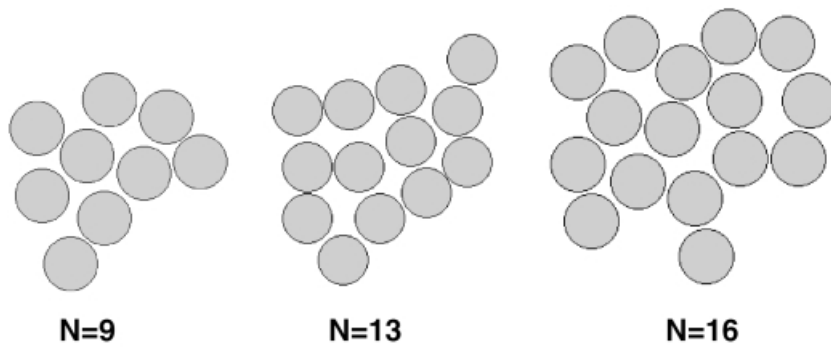
FIGURE 7 Sketch of planar aggregates with $N = 9$, $N = 13$ and $N = 16$ primary particles
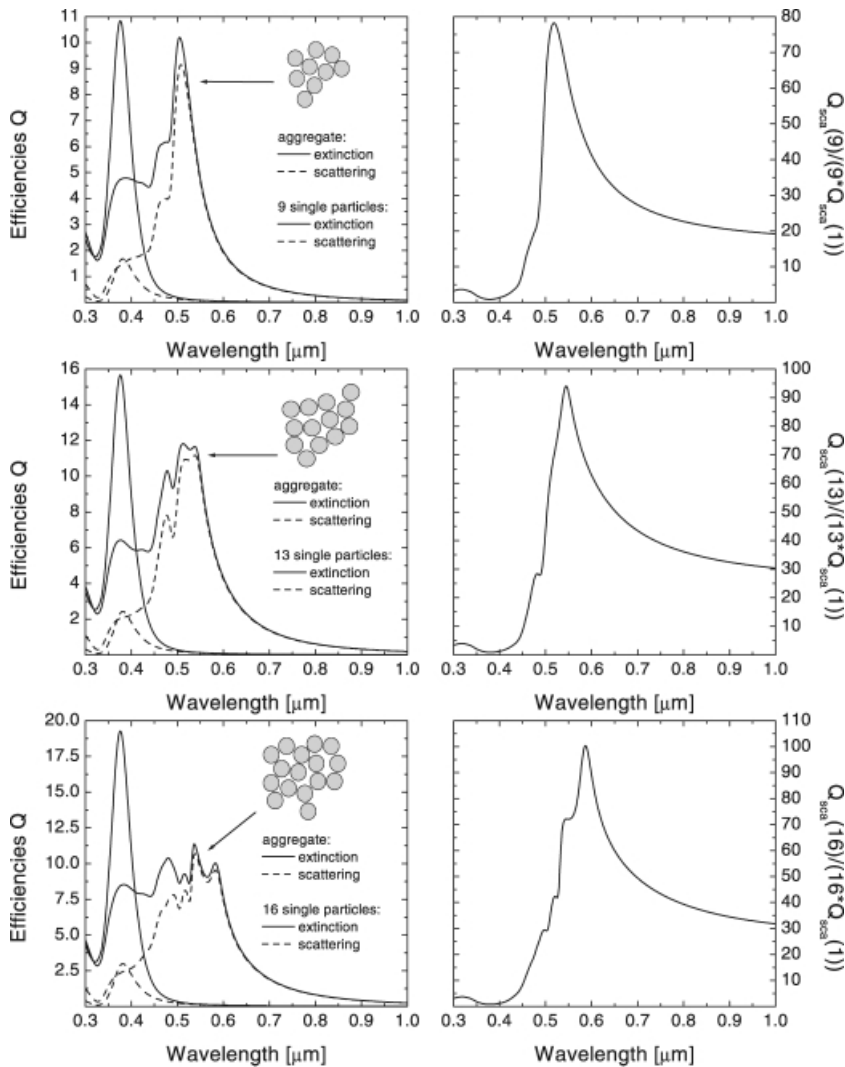

FIGURE 8 Efficiency spectra *(left side)* and scattering enhancement *(right side)* of planar aggregates of silver nanoparticles with diameter $2a = 50$ nm

of which is proportional to the number of particles in the aggregate. However, the strengths of these resonances are different, depending on size and topology of the aggregate. Hence, only a few resonances finally contribute to the extinction and scattering spectra of the aggregate. For an extended discussion of the differences in light scattering by isolated single nanoparticles or by aggregates, it is useful to introduce the scattering enhancement, defined by the ratio $Q_{sca}(N)/(N^* Q_{sca}(1))$. It is shown on the right side of Fig. 8. The scattering enhancement for the considered aggregates is minimum 20 ($N = 9$) and is peaked at a wavelength λ_0

that is dependent upon the number N of primary particles. For $N = 9$ it is $\lambda_0 = 519$ nm and the enhancement amounts to 78, for $N = 13$ it is $\lambda_0 = 545$ nm and the enhancement amounts to 94, and for $N = 16$ it is $\lambda_0 = 587$ nm and the enhancement amounts to 100. This means that already in the far-field zone the scattering of light by these aggregates exceeds the scattering by N isolated particles by a factor of 80–100 at λ_0. Compared to one single particle the enhancement is still larger by the factor N, e.g. it is 1600 for the aggregate with $N = 16$ primaries. The maximum enhancement shifts to longer wavelengths with increasing aggregate
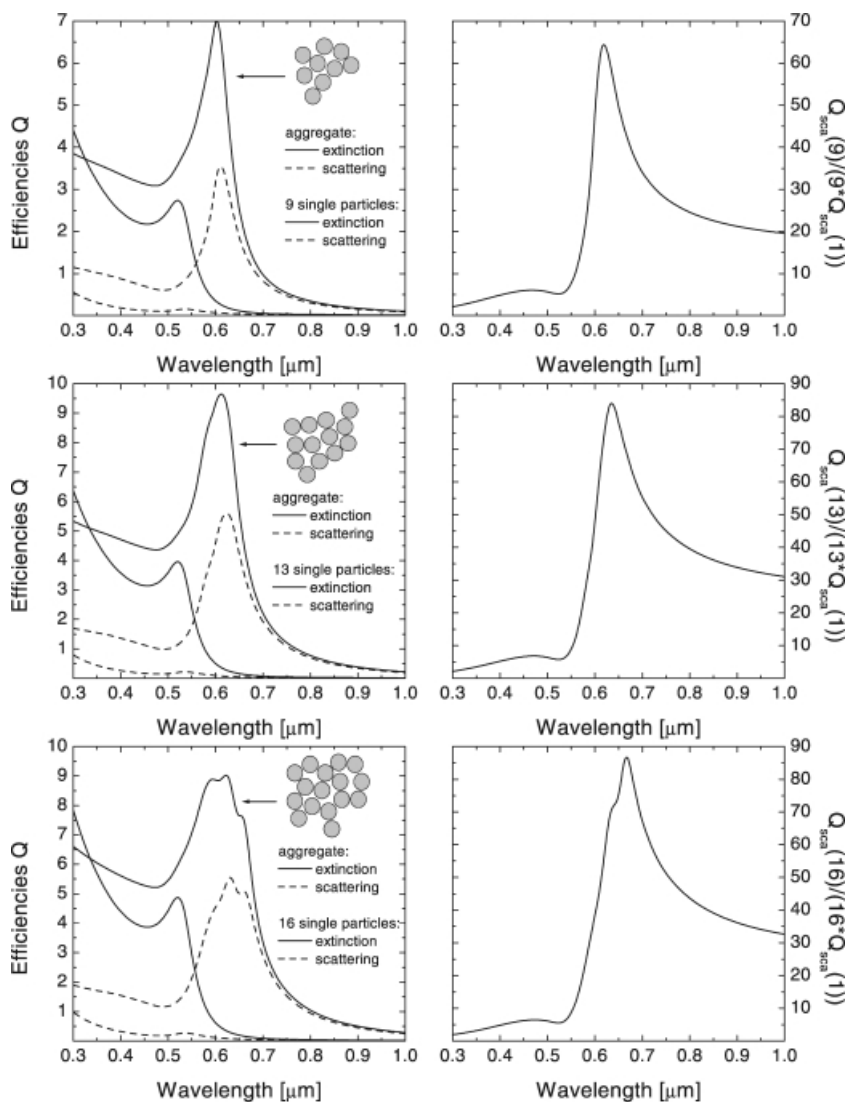
FIGURE 9   Efficiency spectra *(left side)* and scattering enhancement *(right side)* of planar aggregates of gold nanoparticles with diameter $2a = 50$ nm
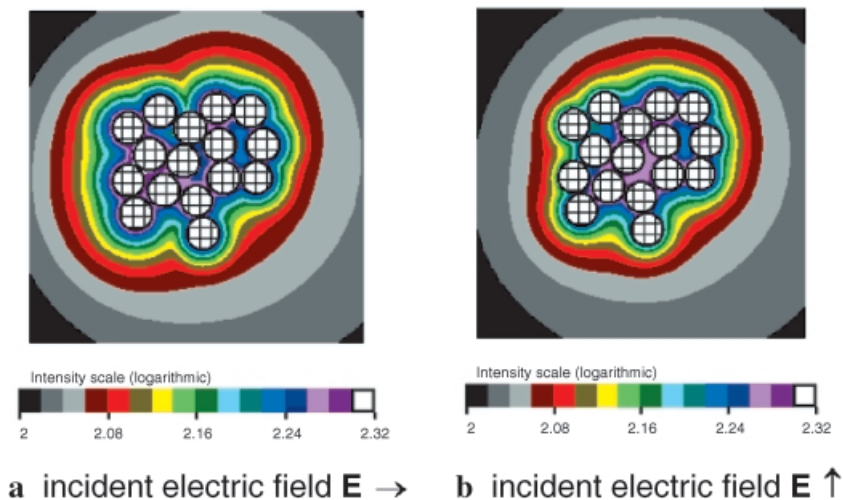

FIGURE 10   Near-field intensities in the equatorial plane *(x–y-*plane) of the planar aggregate with $N = 16$ Au particles for an incident wave propagating along the *z*-axis, being polarized. **a** Along the *x*-axis. **b** Along the *y*-axis

size. Nevertheless, we point to the fact that this shift will run into saturation for large aggregates. This is because the particles in an aggregate interact via the scattered waves. Their amplitudes, however, decrease with increasing distance. For a sufficiently large distance between two particles – amount-

ing to at least 5 primary particle diameters – the interaction becomes negligible.

For aggregates of gold nanoparticles the extinction spectra in Fig. 9 are similar to those of silver aggregates in Fig. 8 except that the resonances of the aggregates are less resolved

than for silver. Only one broadened extinction peak can be observed that is shifted to longer wavelengths. The peak position, and in consequence also the peak in the scattering enhancement, shifts to longer wavelengths with increasing aggregate size. The corresponding values for λ_0 and the peak magnitude are $\lambda_0 = 619$ nm with magnitude 64 for $N = 9$, $\lambda_0 = 634$ nm and magnitude 84 for $N = 13$, and $\lambda_0 = 667$ nm with magnitude 87 for $N = 16$. The minimum enhancement amounts to 20 compared to N primary particles.

In turning to the discussion of the spatial distribution of the near-field intensities, we restrict ourselves to the aggregate of $N = 16$ gold particles. For this aggregate the intensity of the scattered light in the vicinity of the 16 primary particles is calculated at $\lambda = 830$ nm in the equatorial plane, which is in the present case the x–y-plane. The results are depicted in Fig. 10 for a plane incident wave propagating along the positive z-axis of a reference frame centered in one particle of the aggregate and being polarized either along the x-axis (Fig. 10a) or along the y-axis (Fig. 10b). The hatched spherical regions correspond to the nanoparticles. The intensities are plotted with a logarithmic scale. Comparing with the results in Fig. 5, some similarities with the near-field scattering by a single particle can be recognized for the scattering intensities outside the aggregate. The aggregate as a whole just behaves similar to a larger single particle whose size is still small compared to the wavelength $\lambda = 830$ nm as the dipole radiation dominates the scattering intensities. In between the particles, however, the constructive interference of all scattered fields yields distinct regions where the near-field intensities are particularly large. The location of these "hot spots" depends on the polarization of the incident light, which can be recognized when comparing Figs. 10a and 10b. For the electric field parallel to the x-axis the hot spot includes the seven leftmost particles in the aggregate, whereas for the electric field parallel to the y-axis, the hot spot is centered in the aggregate and includes six particles. Comparing the intensity in the hot spots with the near-field intensities at the surface of a single particle with $2a = 50$ nm (not presented here), the intensity in the hot spot is increased by a factor of 37, which exceeds a factor of 16 coming from the number of primaries in the aggregate.

Aggregation of nanoparticles has been experimentally found to be essential also in SERS to realize large Raman signals [5, 17]. A few first theoretical treatments [18, 19] and some recent works [20, 21] already gave qualitative agreement with experimental results and also yield "hot spots" in dependence on size and topography of the aggregates and on the polarization of the incident light [20, 21]. However, these works are based on the coupling of dipoles, i.e. the primary particles in the aggregates are assumed to be small compared to the wavelength of light and also the radiated fields of the particles are approximated by only dipole radiation. This is a serious restriction compared with the analytical solution of light scattering by aggregates presented above. Hence, a quantitative determination of Raman intensities remains difficult from the coupled-dipole approximation. Markel et al. [21] give an estimation also for the near-field intensity in the "hot spots", showing that it can exceed a factor of 10^5. They conclude that with these local fields, SERS enhancements of 10^{10} can be achieved. A more quantitative analysis, how-

ever, is missing. In contrast, we find from our calculations that at wavelengths in common SERS experiments (780 nm, 830 nm) the enhancement of the far-field intensity of the elastically scattered light of the considered aggregates amounts to $\approx 180\,(N = 9) - 640\,(N = 16)$ compared to one single particle for silver or gold particle aggregates of particles with $2a = 50$ nm. From the analysis of the near-field intensities we obtain a further enhancement by a factor of 37 in the "hot spots" for the aggregate with $N = 16$ primary particles. That means that we obtain a total enhancement of the intensity in elastic light scattering amounting to 24 000 in the "hot spots". This is only a factor 4 smaller than the estimation in [21], but also shows that enhancements of at least 10^8 can be obtained in SERS when using the appropriate single particles and aggregates. The advantage of our approach is that we can calculate near-field and far-field intensities of aggregates beyond the coupled-dipole approach, i.e. also for larger primary particles.

5   Summary

We have discussed the differences between the near-field and the far-field scattering of light by small particles. The behavior of the scattered wave in the near-field of the scatterer is very important in, e.g. surface enhanced Raman scattering (SERS) or for near-field optical microscopy.

Whereas Messinger et al. [13] discussed the wavelength dependence of the near-field efficiencies Q_{NF} and Q_R at distance $R = a$, i.e. at the surface of the particle with diameter $2a$, in this paper the discussion has been extended to the distance dependence. It has been shown that the contribution of the radial field component becomes negligible for distances $R \geq 10a$ and Q_{NF} tends to the limiting value Q_{sca}, the far-field scattering efficiency according to the Mie theory. In the vicinity of the cluster, however, the radial component of the electric field determines the electric field, leading to strongly enhanced fields. The contribution of Q_R to Q_{NF} amounts to 67% at the surface of a nanoparticle. As Q_{NF} and Q_R represent the square of either the spatially averaged total electric field of the scattered wave, or the spatially averaged radial component E_r of the electric field of the scattered wave, no information about the angular distribution of the intensity of the scattered light is contained in these quantities. Therefore, phase functions that describe the angular distribution of the scattered light are introduced in the near-field and have been discussed in comparison with the far-field scattering intensities in the plane of incidence and perpendicular to the plane of incidence according to the Mie theory. It has been shown that the contributions of E_θ and E_φ of the scattered electric field are similar to the far-field, except that the magnitude of the corresponding intensities are increased by a factor 7 close to the particle surface. At distances $R = 5a$, the intensities are of comparable magnitude as in the far-field. However, the component E_r leads to striking differences for the intensity in the plane of incidence, as $|E_r|^2$ only contributes to this intensity. For a small particle that can be described in the far-field by a scattering dipole, the intensity of the scattered light in the plane of incidence is proportional to $(\cos\theta)^2$, having minima at scattering angles given by $\theta = \pm 90°$. In contrast, in the near-field these minima have vanished due to $|E_r|^2$, which ap-

pears to be perpendicular to $|E_\theta|^2$ in the plane of incidence, and the intensity at $\theta = \pm 90°$ is even larger than that at $\theta = 0°$ and $\theta = 180°$.

In a second part, we have extended the discussion to aggregates of spherical particles, for which the electromagnetic interaction in the near-field leads to striking effects in the scattering and absorption already in the far-field. At long wavelengths, where the surface plasmon peak in the scattering and absorption of light by a single particle is strongly decreased, the aggregates exhibit strong spectral features mainly in the scattering. In this wavelength region the far-field scattering by an N-particle aggregate is enhanced by a minimum factor of about 20 compared to the scattering by N isolated particles. Larger enhancements of $\approx 60-100$ can also be obtained at distinct wavelengths where the ratio (scattering of an N-particle aggregate)/(scattering of N isolated particles) is peaked. The wavelength of this maximum depends on the particle material and the number N of primary particles in the aggregate. It shifts to longer wavelengths with increasing N. For the considered silver aggregates, it ranges approximately between 500 nm and 600 nm, and for the considered gold aggregates between 600 nm and 700 nm. In the near-field intensities, "hot spots" appear between particles in the aggregate where the near-field intensity is particularly large, with additional enhancements by a factor of approximately 40. The total enhancement of the elastically scattered light amounts to a minimum of 10^4 for aggregates of appropriate size of about $15-20$ primary particles. If the inelastically scattered light in SERS is resonant with these local fields, therefore, enhancements of the Raman intensity in SERS of a minimum of 10^8 can be achieved, which is in agreement with estimations from

a coupled-dipole approximation [21]. However, the advantage of our approach is that we can determine near-fields and far-fields beyond the dipole approximation, i.e. also for larger primary particles.

REFERENCES

1 RK. Chang, T.E. Furtak: *Surface Enhanced Raman Scattering* (Plenum Press, New York 1982)

2 A. Otto: In *Light Scattering in Solids*, Vol. IV, ed. by M. Cardona, G. Güntherodt (Springer-Verlag, Berlin, Heidelberg 1984)

3 M. Moskovits: Rev. Mod. Phys. **57**, 783 (1985)

4 M. Stockman, M. Shalaev, M. Moskovits, R. Botet, T.F. George: Phys. Rev. B **46**, 2821 (1992)

5 K. Kneipp, Y. Wang, H. Kneipp, I. Itzkan, R.R. Dasari, M.S. Feld: Phys. Rev. Lett. **78**, 2444 (1996)

6 R. Neuendorf, M. Quinten, U. Kreibig: J. Chem. Phys. **104**, 6348 (1996)

7 M. Quinten, A. Leitner, J.R. Krenn, F.R. Aussenegg: Opt. Lett. **23**, 1331 (1998)

8 J.R. Krenn, R. Wolf, A. Leitner, F.R. Aussenegg: Opt. Commun. **137**, 46 (1997)

9 M. Quinten, A. Pack, R. Wannemacher: Appl. Phys. B **68**, 87 (1998)

10 R. Wannemacher, A. Pack, M. Quinten: Appl. Phys. B **68**, 225 (1998)

11 M. Quinten: Appl. Phys. B **70**, 579 (2000)

12 G. Mie: Ann. Phys. (Leipzig) **25**, 377 (1908)

13 B.J. Messinger, K.U. von Raben, R.K. Chang, P.W. Barber: Phys. Rev. B **24**, 649 (1981)

14 M. Quinten.: Z. Phys. D **35**, 217 (1995)

15 J.M. Gérardy, M. Ausloos: Phys. Rev. B **25**, 4204 (1982)

16 M. Quinten: Z. Phys. B **101**, 211 (1996)

17 C.G. Blatchford, J.R. Campbell, J.A. Creighton: Surface Sci. **120**, 435 (1982)

18 P. Clippe, R. Evrard, A.A. Lucas: Phys. Rev. B **14**, 1715 (1976)

19 M. Ausloos, P. Clippe, A.A. Lucas: Phys. Rev. B **18**, 7176 (1978)

20 S.I. Bozhevolnyi, V.A. Markel, V. Coello, W. Kim, V.M. Shalaev: Phys. Rev. B **58**, 11441 (1998)

21 V.A. Markel, V.M. Shalaev, P. Zhang, W. Huynh, L. Tay, T.L. Haslett, M. Moskovits: Phys. Rev. B **59**, 10903 (1999)